Available online at www.sciencedirect.com
SCIENCE DIRECT
Journal of Solid State Chemistry 179 (2006) 974–984
JOURNAL OF SOLID STATE CHEMISTRY
www.elsevier.com/locate/jssc

# Effect of sintering on the ionic conductivity of garnet-related structure $Li_5La_3Nb_2O_{12}$ and In- and K-doped $Li_5La_3Nb_2O_{12}$

Venkataraman Thangadurai*, Werner Weppner

*Chair for Sensors and Solid State Ionics, Faculty of Engineering, University of Kiel, Kaiserstr. 2, D 24143-Kiel, Germany*

Received 12 July 2005; received in revised form 20 October 2005; accepted 11 December 2005
Available online 20 January 2006

**Abstract**

Garnet-structure related metal oxides with the nominal chemical composition of $Li_5La_3Nb_2O_{12}$, In-substituted $Li_{5.5}La_3Nb_{1.75}In_{0.25}O_{12}$ and K-substituted $Li_{5.5}La_{2.75}K_{0.25}Nb_2O_{12}$ were prepared by solid-state reactions at 900, 950, and 1000 °C using appropriate amounts of corresponding metal oxides, nitrates and carbonates. The powder XRD data reveal that the In- and K-doped compounds are isostructural with the parent compound $Li_5La_3Nb_2O_{12}$. The variation in the cubic lattice parameter was found to change with the size of the dopant ions, for example, substitution of larger $In^{3+}$ ($r_{CN6}$: 0.79 Å) for smaller $Nb^{5+}$ ($r_{CN6}$: 0.64 Å) shows an increase in the lattice parameter from 12.8005(9) to 12.826(1) Å at 1000 °C. Samples prepared at higher temperatures (950, 1000 °C) show mainly bulk lithium ion conductivity in contrast to those synthesized at lower temperatures (900 °C). The activation energies for the ionic conductivities are comparable for all samples. Partial substitution of $K^+$ for $La^{3+}$ and $In^{3+}$ for $Nb^{5+}$ in $Li_5La_3Nb_2O_{12}$ exhibits slightly higher ionic conductivity than that of the parent compound over the investigated temperature regime 25–300 °C. Among the compounds investigated, the In-substituted $Li_{5.5}La_3Nb_{1.75}In_{0.25}O_{12}$ exhibits the highest bulk lithium ion conductivity of $1.8 \times 10^{-4}$ S/cm at 50 °C with an activation energy of 0.51 eV. The diffusivity (''component diffusion coefficient'') obtained from the AC conductivity and powder XRD data falls in the range $10^{-10}$–$10^{-7}$ $cm^2/s$ over the temperature regime 50–200 °C, which is extraordinarily high and comparable with liquids. Substitution of Al, Co, and Ni for Nb in $Li_5La_3Nb_2O_{12}$ was found to be unsuccessful under the investigated conditions.


*Keywords:* Synthesis; Structure; AC impedance; Ionic conductivity; $Li_5La_3Nb_2O_{12}$; In- and K-doped $Li_5La_3Nb_2O_{12}$; Garnets; Lithium; Solid electrolytes

## 1. Introduction

Solid-state lithium ion conductors (SSLICs) have recently drawn much attention due to their possible potential application in all-solid-state rechargeable (secondary) batteries and also in other solid-state electrochemical devices that include sensors for various gases (e.g., CO, $CO_2$, $NO_x$) and electrochromic displays [1–5]. Solid electrolytes with a high $Li^+$-ion conductivity, stability against chemical reactions with elemental Li (or Li-metal alloy) negative (anode) and Co-, Ni- or Mn-containing positive (cathode) electrodes, and decomposition voltages higher than 5.5 V vs. elemental Li are especially useful to achieve high energy densities and long-term stability. All-solid-state lithium batteries are believed to have remarkable advantages over already commercialized lithium ion batteries utilizing aprotic solutions or gel electrolytes with regard to battery miniaturization, high-temperature operation, thermal shock resistance and solving the battery safety problems by completely replacing the organic based liquid/gel electrolytes [1,6,7].

Recently, we have reported a novel class of fast lithium ion conducting metal oxides with the nominal chemical composition of $Li_5La_3M_2O_{12}$ ($M$ = Nb, Ta) possessing garnet-related structure [8–11]. The bond valence analysis of $Li^+$-ion distribution confirms transport pathways, which relate to the experimentally observed high $Li^+$-ion conductivity. The $Li^+$-ions move in a three-dimensional (3D) network of energetically equivalent partially occupied sites [11]. $Li_5La_3M_2O_{12}$ ($M$ = Nb, Ta) are the first

*Corresponding author. Department of Chemistry, University of Calgary, 2500 University Dr. NW, Calgary, Alberta, Canada T2N 1N4. Fax. +1 403 289 9488/+49 431 880 6203.
*E-mail addresses:* vt@tf.uni-kiel.de, vthangad@ucalgary.ca (V. Thangadurai).

0022-4596/$ - see front matter © 2005 Elsevier Inc. All rights reserved.
doi:10.1016/j.jssc.2005.12.025

examples of fast lithium ion conductors possessing garnet-like structure and give rise to further investigations of conductivity optimization by chemical substitutions and structural modifications.

Based on bond valence analysis of $Li_5La_3M_2O_{12}$ [11], we expected that the aliovalent substitutions at the La- and Nb-sites will significantly modify the connectivity of the network by controlling the number of easily accessible vacancies, and, hence, conductivity could be tailored further by appropriate chemical doping. Accordingly, in our previous study, we have shown that partial substitution of divalent alkaline earth ions for a trivalent La in $Li_5La_3M_2O_{12}$ ($M = Nb$, Ta) yields a novel series of garnet-like structure compounds with the general chemical formula of $Li_6ALa_2M_2O_{12}$ ($A = Ca$, Sr, Ba) [12,13]. Among the investigated compounds, the $Li_6BaLa_2Ta_2O_{12}$ showed the highest $Li^+$-ion conductivity of $4 \times 10^{-5}$ S/cm at 22 °C with an activation energy of 0.40 eV [13].

In the present contribution, we explore new chemical substitutions in $Li_5La_3Nb_2O_{12}$ for further understanding the composition–structure–electrical conductivity relationships and also to investigate the electrical properties under different sintering conditions. Partial substitution of trivalent La by monovalent K and pentavalent Nb by trivalent In yields a new members of garnet-like structure $Li_5La_3Nb_2O_{12}$. A comparison of lithium ion conductivity of K- or In-doped $Li_5La_3Nb_2O_{12}$ with the parent compound will be presented and the effect of synthesis/sintering conditions on the transport properties will be described.

## 2. Experimental section

### 2.1. Synthesis and phase characterization

Conventional solid-state reaction procedure was employed to prepare the garnet-like compounds. Required amounts of a high purity (>99%) chemicals $Li_2CO_3$, $La_2O_3$ (pre-dried at 900 °C for 24 h), $Nb_2O_5$, $KNO_3$, $In_2O_3$, $Al(NO_3)_3 \cdot 9H_2O$, $Co(NO_3)_2 \cdot 6H_2O$, and $NiCO_3$ obtained from Sigma-Aldrich/Fluka (Taufkirchen, Germany)/Chempur (Karlsruhe, Germany) were mixed in 2-propanol and ball milled using zirconia balls for 12 h. After the evaporation of solvents at room temperature, the mixtures were heated at 700 °C in air for 12 h and then cooled down to room temperature. The resultant powders were ground again for another 12 h using 2-propanol and heated at elevated temperatures (900–1000 °C) with an heating and cooling rate of ~5 °C/min. Table 1 lists the sintering conditions employed in the present investigations. In the final stage of heat treatment, the reaction products were pressed into pellets by isostatic pressure. To compensate for the loss of lithium and potassium during the sintering, 10 wt% excess amount of $Li_2CO_3$ and $KNO_3$ was added. The sintered pellets were cut into small pellets using diamond saw. Pellets were ground for phase characterization employing X-ray powder diffraction (XRD) (SEIFERT 3000, Cu$K\alpha$, Germany) at room temperature. The lattice constant was determined from powder XRD data by least-squares refinement. A scanning electron microscope (SEM) (PHILIPS SEM XL 30 electron microscope, The Netherlands) was used to monitor the surface morphology of the sample pellets.

### 2.2. Electrical characterization

The electrical conductivity of the prepared garnet-like structure sample pellets (~0.1–0.22 cm in thickness; ~0.8–1 cm in diameter) were measured in air by using $Li^+$-ion blocking Au-electrodes (Au paste cured at 700 °C for 2 h) in the temperature range from 25 to 300 °C by employing an HP 4192 A Impedance and Gain-Phase Analyzer (5 Hz−13 MHz) interfaced with a PC. A two-probe cell was used for these measurements. Prior to each impedance measurement, the samples were equilibrated for 2–48 h at constant temperature. All measurements were made during both heating and cooling cycles.

Table 1
Summary of chemical compositions, sample acronym, synthesis conditions, and electrical conductivity data of investigated garnet-related structure metal oxides

| Compound | Sample acronym | Synthesis conditions ($T$ °C/time h) | $\sigma_{50\,°C}$ (S/cm) | $\sigma_{200\,°C}$ (S/cm) | $E_a$ (eV) |
|---|---|---|---|---|---|
| $Li_5La_3Nb_2O_{12}$ | LLNO-1 | 700/12; 900/12 | $5.7 \times 10^{-6}$ | $2.0 \times 10^{-3}$ | 0.56 |
| | LLNO-2 | 700/12; 800/12; 950/24 | $2.3 \times 10^{-5}$ | $5.7 \times 10^{-3}$ | 0.55 |
| | LLNO-3 | 700/12; 800/12; 1000/24 | $4.4 \times 10^{-5}$ | $1.5 \times 10^{-2}$ | 0.55 |
| $Li_{5.5}La_3Nb_{1.75}In_{0.25}O_{12}$ | LLNIO-1 | 700/12; 850/12; 900/24 | $1.4 \times 10^{-5}$ | $5.3 \times 10^{-3}$ | 0.49 |
| | LLNIO-2 | 700/12; 850/12; 950/24 | $1.8 \times 10^{-4}$ | $3.5 \times 10^{-2}$ | 0.51 |
| | LLNIO-3 | 700/12; 850/12; 1000/24 | $1.0 \times 10^{-4}$ | $2.4 \times 10^{-2}$ | 0.52 |
| $Li_{5.5}La_{2.75}K_{0.25}Nb_2O_{12}$ | LLKNO-1 | 700/12; 850/12; 900/24 | $2.5 \times 10^{-5}$ | $6.2 \times 10^{-3}$ | 0.53 |
| | LLKNO-2 | 700/12; 850/12; 950/24 | $6.0 \times 10^{-5}$ | $1.4 \times 10^{-2}$ | 0.49 |
| | LLKNO-3 | 700/12; 850/12; 1000/24 | $6.0 \times 10^{-5}$ | $1.4 \times 10^{-2}$ | 0.49 |
| $Li_5La_3Nb_2O_{12}$ | LLNO | 700/6; 900/24 | $4.4 \times 10^{-5}$ | $5.7 \times 10^{-3}$ | 0.43[a] |

[a]Data taken from Ref. [8].

## 3. Results

### 3.1. X-ray powder diffraction

Fig. 1 shows the powder XRD patterns of the parent $Li_5La_3Nb_2O_{12}$ sintered at 900, 950, and 1000 °C together with the standard pattern of $Li_5La_3Nb_2O_{12}$ reported in Joint Committee on Powder Diffraction Standards (JCPDS: 84-1753). We see that the XRD patterns remain nearly the same for all three different temperatures of compound sintering. Partial substitutions of K for La and In for Nb in $Li_5La_3Nb_2O_{12}$ are readily obtained by reacting corresponding metal oxides and carbonates at elevated temperature. Table 2 give the indexed powder XRD patterns of reaction products obtained at 950 °C for $Li_{5.5}La_3Nb_{1.75}In_{0.25}O_{12}$ and $Li_{5.5}La_{2.75}K_{0.25}Nb_2O_{12}$ together with corresponding data of the parent compound $Li_5La_3Nb_2O_{12}$, and confirm the formation of a single-phase garnet-like structures. However, partial replacement of Nb by Co, Ni and Al does not yield single-phase materials under the investigated conditions, albeit such a substitution is well-known in other crystal structures, for example, $ABO_3$ ($A$ = mono, di or trivalent metal ions; $B$ = tri, tetra or pentavalent metal ions) perovskite and perovskite-related structures [14]. Fig. 2 shows the variation of lattice parameter of $Li_5La_3Nb_2O_{12}$, $Li_{5.5}La_3Nb_{1.75}In_{0.25}O_{12}$ and $Li_{5.5}La_{2.75}K_{0.25}Nb_2O_{12}$ as a function of sintering temperature.

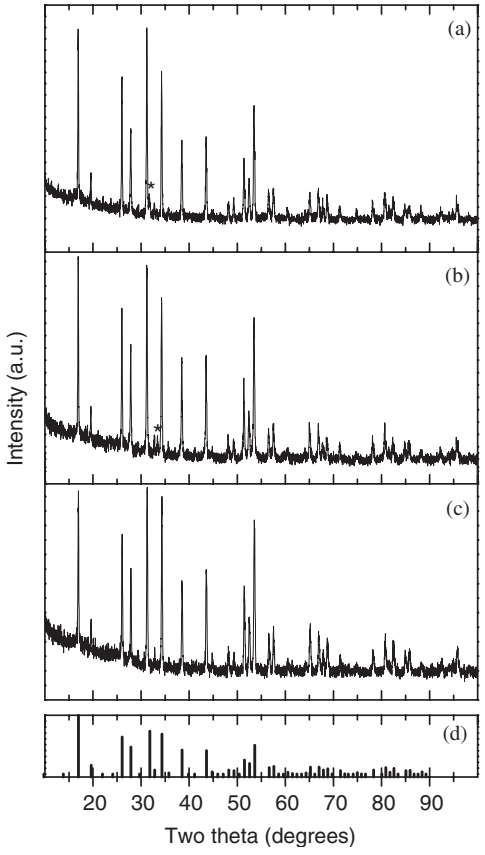


Fig. 1. Powder XRD patterns of $Li_5La_3Nb_2O_{12}$ prepared at (a) 900 °C (LLNO-1), (b) 950 °C (LLNO-2), and (c) 1000 °C (LLNO-3). For comparison, the patterns of JCPDS card No. 84-1753 is shown in (d). *Indicates impurity phase contribution due to the perovskite-like $La_2LiNbO_6$ phase.

### 3.2. AC impedance analysis

Typical impedance plots for the parent compound $Li_5La_3Nb_2O_{12}$ obtained at 55 and 100 °C in air for three different sintering temperatures (900, 950, and 1000 °C) are shown in Fig. 3. We see clearly the large bulk (grain interior, $R_b$) resistance at the high-frequency side, grain boundary ($R_{gb}$) contribution and a tail in the low-frequency regime for the 900 °C sample (Fig. 3a: left hand side). The samples prepared at 950 and 1000 °C show mainly single semicircle contributions in the high-frequency regime and tails at the low-frequency side (Figs. 3b and c). At higher temperature (above ~70 °C), impedance plots of 900 °C parent compound could not be well resolved into bulk, grain boundary and electrode effects. For experimental and practical reasons of applications, we have considered uniformly the total (bulk + grain boundary) contribution for the presentation of the electrical conductivity over a wide range of temperature. In Fig. 4, we give typical impedance data obtained for the In- and K-doped $Li_5La_3Nb_2O_{12}$ at 45 °C. We see a similar conductivity behavior as for the parent compound (Fig. 3). However, it must be mentioned that the bulk impedance contribution of the 1000 °C sample is slightly higher than that of the 950 °C sample for In- and K-substituted materials. 0.5 mol% In- and K-doped samples are highly porous and mechanically weak and crack while cutting the thick pellets after sintering. Thus, further optimization of the synthesis condition is required to measure reliable lithium ion conductivity.

### 3.3. Lithium ion conductivity

The Arrhenius plots for lithium ion conductivity of the parent compound $Li_5La_3Nb_2O_{12}$ and $Li_{5.5}La_3Nb_{1.75}In_{0.25}O_{12}$ and $Li_{5.5}La_{2.75}K_{0.25}Nb_2O_{12}$ prepared at 900, 950, and 1000 °C are shown in Fig. 5. The electrical conductivity data obtained during the heating and the cooling cycle follow the same line, suggesting that the measured values are equilibrium data. We see that the samples prepared at higher temperatures show higher ionic conductivities than the low temperature synthesized materials. The conductivity increases with increasing the sintering temperature for the parent compound $Li_5La_3Nb_2O_{12}$ (Fig. 5a). However, In- and K-doped LLN prepared at 1000 °C show slightly lower (⩽half-order of magnitude) conductivity than 950 °C sintered samples (Figs. 5b and c). The activation energies ($E_a$) for the ionic conductivity were determined from the Arrhenius plots employing the equation:

$$\sigma T = A \exp\left(\frac{-E_a}{kT}\right), \quad (1)$$

Table 2
Indexed powder XRD patterns of parent compound $Li_5La_3Nb_2O_{12}$ prepared at 900 °C (LLNO-1), 950 °C (LLNO-2), 1000 °C (LLNO-3), $Li_{5.5}La_3Nb_{1.75}In_{0.25}O_{12}$ (LLNIO-2), and $Li_{5.5}La_{2.75}K_{0.25}Nb_2O_{12}$ (LLKNO-2) prepared at 950 °C

| | | | LLNO-1 | | | LLNO-2 | | | LLNO-3 | | | LLNIO-2 | | | LLKNO-2 | | |
|---|---|---|---|---|---|---|---|---|---|---|---|---|---|---|---|---|---|
| *h* | *k* | *l* | $d_{obs.}$ (Å) | $d_{cal.}$ (Å) | $I_{ob.}$ | $d_{obs.}$ (Å) | $d_{cal.}$ (Å) | $I_{ob.}$ | $d_{obs.}$ (Å) | $d_{cal.}$ (Å) | $I_{ob.}$ | $d_{obs.}$ (Å) | $d_{cal.}$ (Å) | $I_{ob.}$ | $d_{obs.}$ (Å) | $d_{cal.}$ (Å) | $I_{ob.}$ |
| 2 | 1 | 1 | 5.235 | 5.232 | 100 | 5.235 | 5.233 | 98 | 5.220 | 5.226 | 84 | 5.234 | 5.234 | 100 | 5.223 | 5.222 | 45 |
| 2 | 2 | 0 | 4.531 | 4.531 | 15 | 4.533 | 4.532 | 16 | 4.520 | 4.526 | 15 | 4.526 | 4.532 | 22 | 4.515 | 4.523 | 7 |
| 3 | 2 | 1 | 3.422 | 3.425 | 70 | 3.423 | 3.426 | 78 | 3.419 | 3.421 | 58 | 3.425 | 3.426 | 58 | 3.420 | 3.420 | 32 |
| 4 | 0 | 0 | 3.201 | 3.203 | 43 | 3.201 | 3.205 | 49 | 3.197 | 3.200 | 44 | 3.205 | 3.205 | 41 | 3.200 | 3.200 | 20 |
| 4 | 2 | 0 | 2.864 | 2.865 | 100 | 2.863 | 2.866 | 100 | 2.860 | 2.862 | 100 | 2.865 | 2.866 | 70 | 2.860 | 2.860 | 100 |
| 3 | 3 | 2 | 2.735 | 2.732 | 7 | 2.731 | 2.733 | 8 | 2.725 | 2.729 | 9 | 2.731 | 2.733 | 5 | 2.726 | 2.727 | 4 |
| 4 | 2 | 2 | 2.615 | 2.616 | 77 | 2.615 | 2.617 | 87 | 2.611 | 2.613 | 83 | 2.614 | 2.617 | 75 | 2.609 | 2.611 | 45 |
| 4 | 3 | 1 | 2.518 | 2.513 | 9 | 2.516 | 2.514 | 8 | — | — | — | — | — | — | — | — | — |
| 5 | 1 | 0 | — | — | — | — | — | — | 2.516 | 2.510 | 4 | — | — | — | — | — | — |
| 5 | 2 | 1 | 2.338 | 2.340 | 43 | 2.339 | 2.340 | 56 | 2.336 | 2.337 | 45 | 2.340 | 2.340 | 33 | 2.335 | 2.335 | 25 |
| 6 | 1 | 1 | 2.078 | 2.079 | 45 | 2.079 | 2.080 | 57 | 2.075 | 2.077 | 50 | 2.078 | 2.079 | 33 | — | — | — |
| 6 | 2 | 0 | 2.043 | 2.026 | 6 | 2.024 | 2.029 | 5 | 2.018 | 2.023 | 4 | 2.030 | 2.030 | 7 | 2.022 | 2.022 | 26 |
| 6 | 3 | 1 | 1.889 | 1.889 | 7 | 1.890 | 1.890 | 13 | 1.887 | 1.887 | 11 | 1.890 | 1.890 | 8 | 1.887 | 1.886 | 10 |
| 4 | 4 | 4 | 1.849 | 1.850 | 9 | 1.850 | 1.850 | 11 | 1.846 | 1.848 | 3 | 1.850 | 1.850 | 5 | 1.845 | 1.845 | 5 |
| 6 | 4 | 0 | 1.777 | 1.777 | 33 | 1.777 | 1.778 | 44 | 1.775 | 1.775 | 41 | 1.778 | 1.778 | 24 | 1.773 | 1.774 | 24 |
| 7 | 2 | 1 | 1.743 | 1.744 | 21 | 1.744 | 1.744 | 27 | 1.743 | 1.742 | 27 | 1.743 | 1.744 | 21 | 1.740 | 1.741 | 13 |
| 6 | 4 | 2 | 1.712 | 1.712 | 60 | 1.712 | 1.713 | 83 | 1.709 | 1.710 | 75 | 1.713 | 1.713 | 46 | 1.709 | 1.709 | 48 |
| 1 | 5 | 6 | 1.628 | 1.628 | 14 | 1.627 | 1.628 | 15 | 1.626 | 1.626 | 18 | 1.629 | 1.629 | 15 | 1.625 | 1.625 | 11 |
| 8 | 0 | 0 | 1.600 | 1.601 | 15 | 1.602 | 1.602 | 19 | 1.600 | 1.600 | 22 | 1.606 | 1.603 | 15 | 1.598 | 1.599 | 9 |
| 6 | 5 | 3 | 1.532 | 1.532 | 11 | 1.531 | 1.532 | 5 | 1.528 | 1.530 | 3 | — | — | — | 1.528 | 1.529 | 5 |
| 7 | 5 | 2 | 1.451 | 1.451 | 8 | 1.452 | 1.451 | 6 | 1.449 | 1.449 | 2 | — | — | — | — | — | — |
| 8 | 4 | 0 | 1.432 | 1.433 | 12 | 1.433 | 1.433 | 18 | 1.430 | 1.431 | 22 | 1.433 | 1.433 | 13 | 1.430 | 1.430 | 15 |
| 8 | 4 | 2 | 1.398 | 1.398 | 15 | 1.400 | 1.400 | 19 | 1.400 | 1.400 | 17 | 1.401 | 1.400 | 10 | 1.394 | 1.395 | 11 |
| 9 | 2 | 1 | — | — | — | — | — | — | 1.379 | 1.380 | 8 | — | — | — | — | — | — |
| 7 | 6 | 1 | 1.382 | 1.382 | 8 | 1.382 | 1.382 | 8 | — | — | — | 1.380 | 1.382 | 4 | 1.377 | 1.379 | 4 |
| 6 | 6 | 4 | 1.366 | 1.366 | 11 | 1.366 | 1.367 | 11 | 1.364 | 1.364 | 5 | 1.365 | 1.365 | 9 | 1.364 | 1.363 | 5 |
| 9 | 3 | 2 | 1.322 | 1.322 | 4 | 1.322 | 1.322 | 7 | 1.321 | 1.320 | 6 | 1.323 | 1.322 | 3 | 1.321 | 1.321 | 5 |
| 10 | 1 | 1 | 1.268 | 1.269 | 8 | 1.270 | 1.269 | 3 | 1.270 | 1.267 | 2 | — | — | — | 1.269 | 1.267 | 2 |
| 10 | 3 | 1 | 1.222 | 1.222 | 11 | 1.222 | 1.222 | 10 | 1.222 | 1.220 | 9 | 1.222 | 1.222 | 4 | 1.219 | 1.219 | 5 |
| 10 | 4 | 0 | 1.190 | 1.190 | 11 | 1.190 | 1.190 | 20 | 1.189 | 1.189 | 18 | 1.189 | 1.190 | 12 | 1.188 | 1.188 | 12 |
| 10 | 4 | 2 | 1.170 | 1.170 | 10 | 1.170 | 1.170 | 9 | 1.169 | 1.169 | 13 | 1.170 | 1.170 | 11 | 1.169 | 1.167 | 4 |
| 10 | 5 | 1 | 1.142 | 1.142 | 6 | 1.143 | 1.142 | 9 | 1.141 | 1.140 | 8 | 1.141 | 1.142 | 6 | 1.141 | 1.140 | 5 |
| 8 | 8 | 0 | 1.130 | 1.128 | 5 | — | — | — | 1.131 | 1.131 | 11 | 1.135 | 1.133 | 6 | 1.131 | 1.131 | 7 |
| 9 | 7 | 2 | 1.107 | 1.107 | 4 | 1.107 | 1.107 | 4 | 1.106 | 1.106 | 9 | 1.108 | 1.108 | 3 | 1.105 | 1.105 | 2 |
| 12 | 0 | 0 | 1.069 | 1.068 | 2 | 1.069 | 1.069 | 4 | 1.068 | 1.068 | 4 | 1.072 | 1.075 | 4 | 1.068 | 1.066 | 3 |
| 10 | 7 | 1 | — | — | — | 1.048 | 1.048 | 9 | 1.047 | 1.049 | 5 | — | — | — | — | — | — |
| 12 | 2 | 2 | 1.040 | 1.039 | 11 | — | — | — | 1.038 | 1.038 | 11 | 1.041 | 1.040 | 5 | 1.038 | 1.038 | 4 |
| 9 | 9 | 2 | 0.994 | 0.994 | 4 | 0.996 | 0.996 | 4 | 0.993 | 0.994 | 2 | — | — | — | 0.994 | 0.993 | 3 |
| 12 | 6 | 0 | 0.956 | 0.955 | 7 | 0.956 | 0.956 | 8 | 0.956 | 0.956 | 6 | — | — | — | — | — | — |
| | | | 12.8147(7) Å | | | 12.8189(9) Å | | | 12.8005(9) Å | | | 12.821(2) Å | | | 12.7937(8) Å | | |

where $A$ is the pre-exponential parameter and $k$ is Boltzmann's constant. The electrical conductivity data at 50 and 200 °C are listed together with the activation energies in Table 1.

## 4. Discussion

### 4.1. Structural properties

The garnets are orthosilicate minerals with the general chemical structural formula of $A_3B_2(SiO_4)_3$, where $A$ (divalent alkaline earth ions or trivalent rare earths) and $B$ (transition metal ions) refer to 8- and 6-fold coordinated metal ions sites, respectively [15,16]. $Li_5La_3M_2O_{12}$ ($M$ = Nb, Ta) was found to crystallize in a cubic symmetry with the lattice constant $a = 12.797$ Å for Nb-member and 12.804 Å for Ta-member (Space Group $I2_13$ (No. 199, $Z = 8$)) [9] with an excess of 16 lithium ions per formula unit compared to that of the ideal garnet composition [9,11]. In these compounds, $La^{3+}$ and $M^{5+}$ ions occupy the 8- and 6-fold coordination sites, respectively, and the $Li^+$-ions occupy 6-fold coordination sites (Fig. 6) [9]. The similarity between the structures of the ideal garnet and $Li_5La_3M_2O_{12}$ is that the rare earth ions occupy the dodecahedral (8-fold) coordination site and $M$ atoms occupy the 6-fold coordination site. The main difference is that Si (or other metal ions) in the former case occupy the 4-fold oxygen coordination [12,13] and Li in the latter

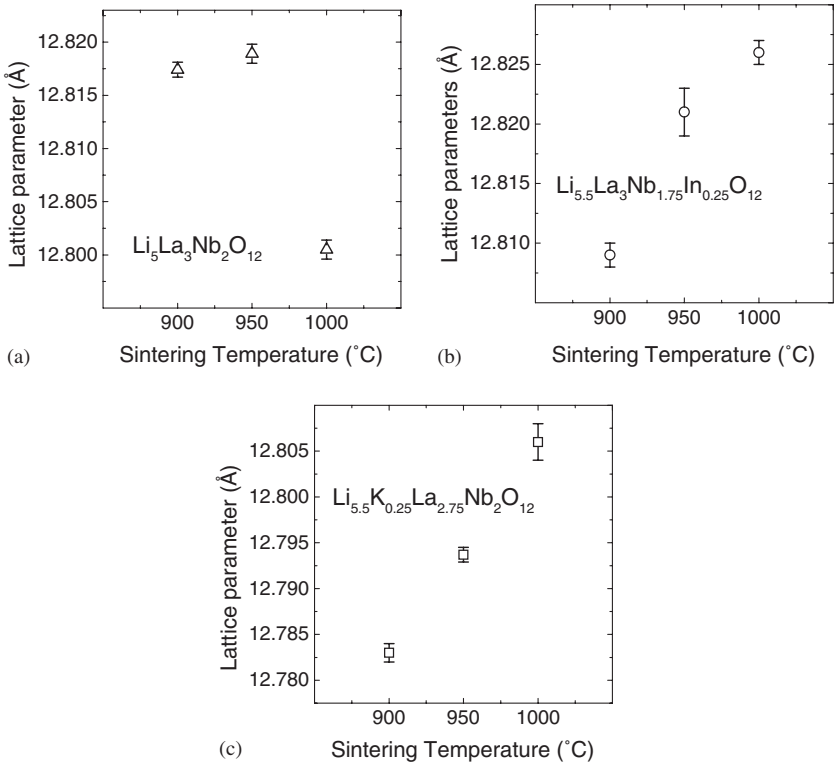


Fig. 2. Sintering temperature dependencies of lattice parameters for garnet-like structured (a) $Li_5La_3Nb_2O_{12}$, (b) $Li_{5.5}La_3Nb_{1.75}In_{0.25}O_{12}$, and (c) $Li_{5.5}La_{2.75}K_{0.25}Nb_2O_{12}$.

case occupies the highly distorted octahedral sites [9]. There are two types of $LiO_6$ octahedras; among them, $Li(I)O_6$ is more distorted than $Li(II)O_6$. $MO_6$ octahedrons are surrounded by six $LiO_6$ octahedra and two lithium-site vacancies cubically. We see that all the investigated compounds crystallize in the parent garnet-like $Li_5La_3Nb_2O_{12}$ structure (Fig. 1 and Tables 1 and 2). The cubic lattice constant increases by substitution of $In^{3+}$ for $Nb^{5+}$, which is consistent with the increasing ionic radii. The 6-coordinated ionic radius increases in the order $Nb^{5+}$ ($r_{CN6}$: 0.64 Å) < $In^{3+}$ ($r_{CN6}$: 0.79 Å) [17]. Since the observed XRD patterns of K- and In-doped samples are similar to that of the parent compound $Li_5La_3Nb_2O_{12}$ (Table 2), we believe that the excess lithium may occupy the empty Li-sites/or any other equivalent interstitial sites in the parent structure [9,11]. However, further experimental studies are required to clarify this aspect.

The lattice parameter was found to increase with increasing sintering temperature for the In- and K-doped samples (Figs. 2b and c), while the parent compound $Li_5La_3Nb_2O_{12}$ (Fig. 2a) show only a slight increase at 950 °C and decreases with further increasing temperature. The slight increase in the lattice parameter of doped materials with increase in the sintering temperature (see for example, LLNIO-1: 12.809(1) Å; LLNIO-2: 12.821(2) Å; LLNIO-3: 12.826(1) Å) may be attributed to the redistribution of metal ions between the surface and the bulk. We speculate that the small amounts of impurity or unreacted metal oxides or metal ions such as K, In, La, and Nb from the surface may enter the bulk at higher temperatures. Accordingly, the bulk composition of materials prepared at three different temperatures may have a small variation in composition. It must be mentioned that a similar observation was reported in the investigation of oxide ion conducing Gd-doped $CeO_2$ in the temperature range 650–1150 °C [18]. It was proposed that as the temperature increases redistribution of Gd between surface and bulk occurs, which slightly increases the fluorite-type structure lattice parameter. The variation in the Ce/Gd ratio between surface and bulk was confirmed by low energy ion scattering (LEIS) and Rutherford backscattering spectroscopy (RBS) investigations [19]. The Ce/Gd ratio changed from 1 at the outermost surface to 4.2 in the bulk.

### 4.2. Electrical properties

#### 4.2.1. AC impedance and microstructure

The appearance of a low-frequency tail in case of ionically blocking electrodes is an indication that the investigated garnet type material is ionic in nature [20–22]. The room temperature impedance plots of samples prepared at low temperature (LLNO-1; LLNIO-1; LLKNO-1) could be well resolved into bulk, grain boundary and electrode resistances corresponding to an equivalent circuit consisting of a series of two parallel

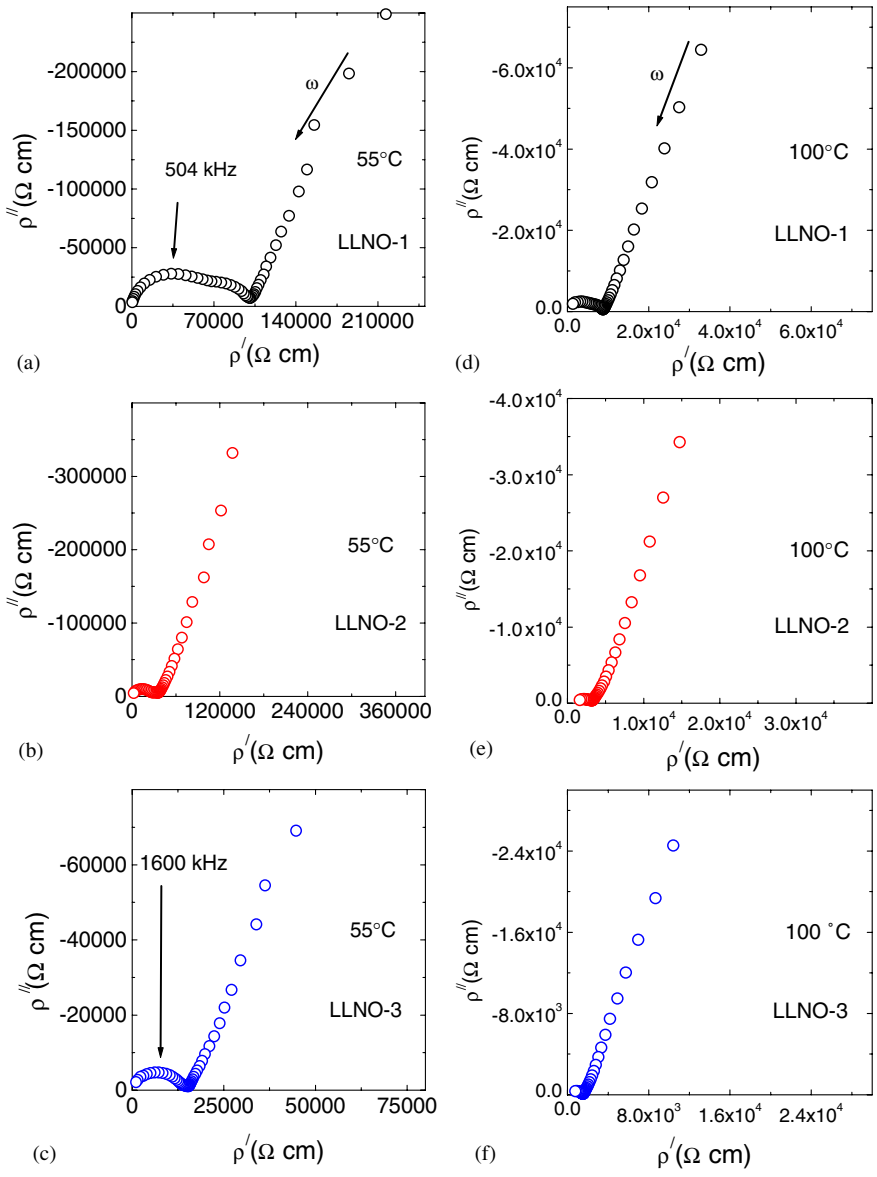


Fig. 3. Typical AC impedance plots obtained in the frequency range 5 Hz–13 MHz using lithium ion blocking Au electrode at 55 °C for $Li_5La_3Nb_2O_{12}$ sintered at (a) 900 °C, (b) 950 °C, and (c) 1000 °C. (d)–(f) Show data at 100 °C for the corresponding compounds.

resistance–capacitance and capacitance contributions $(R_bC_b)(R_{gb}C_{gb})(C_{el.})$ [20–22]. A similar behavior has been observed in our previous study [8,13,14]. The magnitudes of the capacitances of the bulk, grain boundary and electrode interface region were found be in the order of $10^{-12}$, $10^{-8}$, and $10^{-6}$ F, respectively [8,13,14]. These are characteristic values for the bulk, grain boundary and electrode–electrolyte interface contributions of ionically conducting ceramics. The samples prepared at higher temperatures (for example, LLNO-3; LLNIO-2; LLNIO-3; LLKNO-3) exhibit mainly a single parallel resistance–capacitance contribution in the impedance plots. A similar effect was reported recently for lithium ion conducting NASICON-type glass [23] and perovskite-type metal oxides [24] and oxide ion conducting perovskite-type LSGM [25]. In the former case, the lithium ion conductivity increases with increasing sintering time [23] or temperature [24], while in the latter case the grain boundary impedance decreases with increasing grain size [25]. The capacitance ($C$) values obtained from the AC impedance plots (high frequency regime) using the relationship $\omega RC = 1$ ($\omega = 2\pi\nu$; $\nu$ is the frequency and $R$ is the resistance) are nearly the same value (~26–70 pF/cm$^2$), suggesting that the observed semicircle corresponds to the bulk contribution [12,13]. A similar magnitude of bulk capacitance values was reported for other fast lithium ion conductors, e.g., $(Li,La,\square)TiO_3$ [26] ($\square$ = vacancy), $Sr_{0.5}La_{0.05}Li_{0.35}\square_{0.10}Ti_{0.5}Ta_{0.5}O_3$ [27] and $Li_{1+x}Al_xTi_{2-x-y}Ge_y(PO_4)_3$ [28]. However, further study is required to understand the possible contribution of the electronic

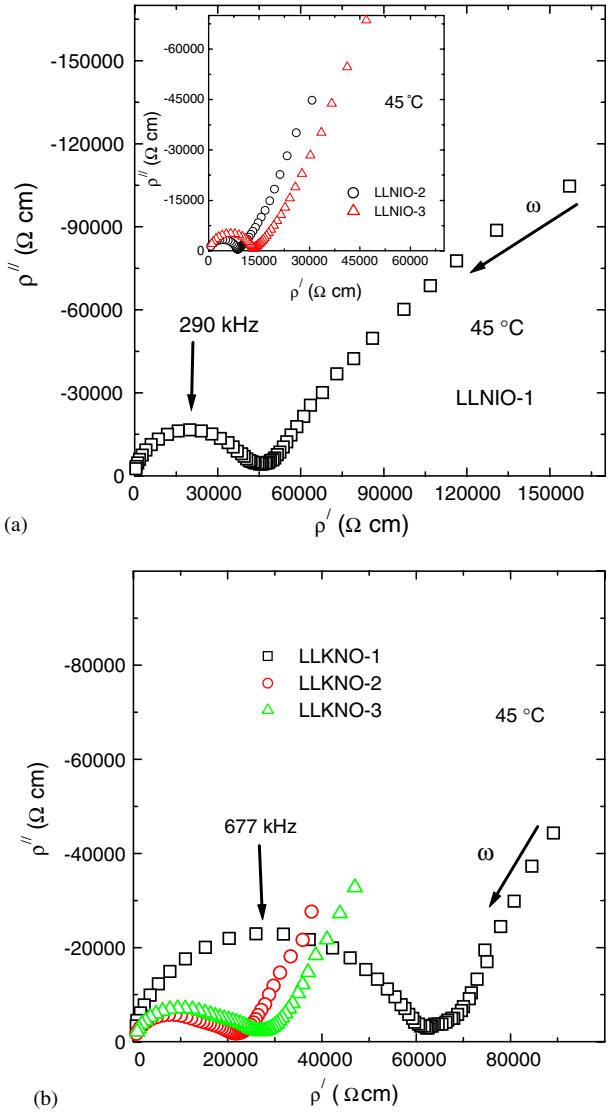


Fig. 4. Typical AC impedance plots obtained in the frequency range 5 Hz–13 MHz using lithium ion blocking Au electrode at 45 °C for (a) $Li_{5.5}La_3Nb_{1.75}In_{0.25}O_{12}$ prepared at 900 °C (LLNIO-1), 950 °C (LLNIO-2), and 1000 °C (LLNIO-3) and (b) $Li_{5.5}La_{2.75}K_{0.25}Nb_2O_{12}$ prepared at 900 °C (LLKNO-1), 950 °C (LLKNO-2), and 1000 °C (LLKNO-3).

conductivity due small polaron mechanism via Nb and Nb/In cations in the parent and K- or In-doped garnet-like structures.

In order to understand the difference in the impedance plots under different sintering conditions, we have performed SEM studies. Fig. 7 shows the SEM images of $Li_5La_3Nb_2O_{12}$ prepared at 900 °C (LLNO-1), 950 °C (LLNO-2), and 1000 °C (LLNO-3). We see that the grain size increases with increasing sintering temperature. Accordingly, the increase of the particle size may be related to the absence of grain-boundary resistance in the impedance plots. A similar effect has been reported for the LSGM samples [25]. For example, LSGM prepared at higher temperature resulted in large grain-size particles and show small grain-boundary resistance compared to that of the low temperature sized products. However, the bulk ionic conductivity was found to be the same for different sintering conditions [25]. In the present investigation we see clearly that not only the grain-boundary contribution but also the bulk-resistance changes with sintering temperature (Fig. 3), which may be attributed to the change in the microstructure.

### 4.2.2. Lithium ion conductivity

In Fig. 8, we compare the best lithium ion conducting $Li_5La_3Nb_2O_{12}$ sample (LLNO-3) sintered at 1000 °C and In- or K-doped samples (LLNIO-2 and LLKNO-2) prepared at 950 °C. We see that the In-substituted compound LLNIO-2 exhibits the highest bulk lithium ion conductivity of $1.8 \times 10^{-4}$ S/cm at 50 °C with an activation energy of 0.51 eV. For single-phase lithium containing materials, the ionic conductivity is given by the equation

$$\sigma = |z_{Li}| q N_{Li} \mu_{Li}, \quad (2)$$

where $z$ is the valence of $Li^+$ ion ($z = 1$ for lithium), $q$ is the elementary charge ($1.6 \times 10^{-19}$ C), $N$ is the concentration of $Li^+$ ions per $cm^3$ and $\mu_{Li}$ is the electrical mobility of $Li^+$ ions. Accordingly, the lithium ion conductivity depends on the concentration of mobile lithium ions and its mobility. The Nernst–Einstein equation gives the relationship between the diffusivity $D$ ("component diffusion coefficient") [29,30] and mobility of lithium at temperature $T$

$$\mu = \frac{|z_{Li}| q D}{kT}. \quad (3)$$

Substitution of Eq. (3) into Eq. (2) gives the relationship between the conductivity and diffusivity

$$\sigma = \frac{q^2 D N}{kT}. \quad (4)$$

The concentration $N$ of lithium ions may be calculated using the powder XRD data employing the equation:

$$N = \frac{1}{V} \times n, \quad (5)$$

where $V$ is the volume of the unit cell and $n$ is the number of lithium ions per unit cell. The concentration of lithium ions in case of the nominal chemical compositions $Li_5La_3Nb_2O_{12}$, $Li_{5.5}La_3Nb_{1.75}In_{0.25}O_{12}$, and $Li_{5.5}La_{2.75}K_{0.25}Nb_2O_{12}$ is $1.902 \times 10^{22}$, $2.088 \times 10^{22}$, and $2.101 \times 10^{22}$ atoms/$cm^3$, respectively. It is assumed that all the lithium ions contribute to the conductivity. Accordingly, the diffusivity obtained from Eq. (4) using the AC conductivity data (Table 1) falls in the range $10^{-10}$–$10^{-7}$ $cm^2/s$ over the temperature regime 50–200 °C and the electrical mobility calculated using Eq. (3) is found to be $10^{-9}$–$10^{-6}$ $cm^2/V\,s$. The high ionic conductivity of doped samples may be due to the slight variation in the concentration of mobile lithium ions and also due to the small change in the lattice parameter compared to that of the parent compound (Fig. 2).

The activation energy for the lithium ion conductivity falls in the range 0.49–0.56 eV for our samples investigated

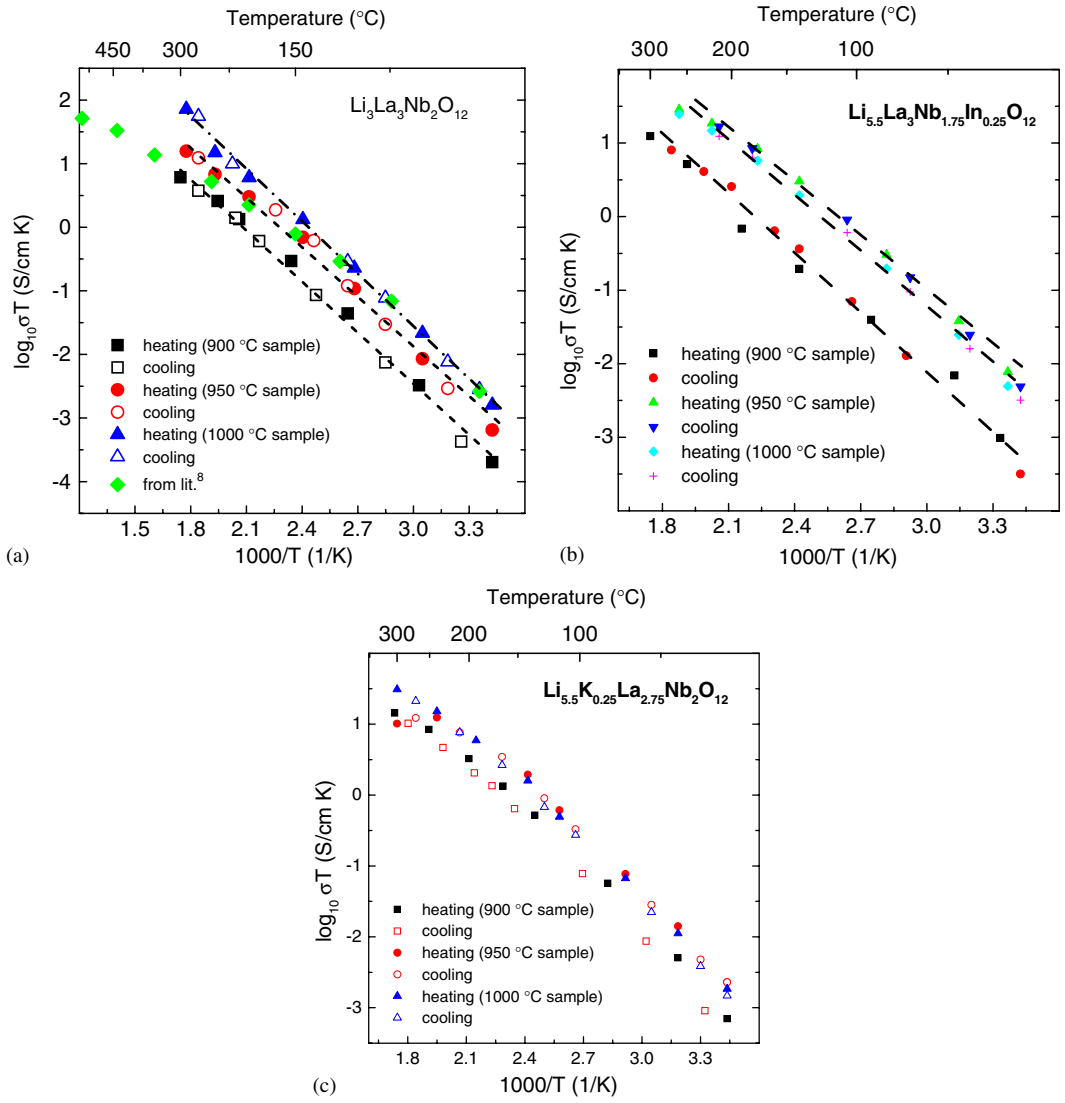


Fig. 5. Arrhenius plots of the total conductivity of (a) $Li_5La_3Nb_2O_{12}$, (b) $Li_{5.5}La_3Nb_{1.75}In_{0.25}O_{12}$, and (c) $Li_{5.5}La_{2.75}K_{0.25}Nb_2O_{12}$. For comparison, the data from literature are included in (a) [8]. The broken line passing through the data points are guides to the eye. We see that the $Li_5La_3Nb_2O_{12}$ prepared at 1000 °C show higher electrical conductivity than those prepared at 900 and 950 °C over the investigated temperature range.

in the present study (Table 1). The activation energy for the electrical conductivity decreases with increasing sintering temperature of the parent compound $Li_5La_3Nb_2O_{12}$ (Fig. 9a) and K-doped $Li_{5.5}La_{2.75}K_{0.25}Nb_2O_{12}$ (Fig. 9c). The In-substituted compound $Li_{5.5}La_{2.75}K_{0.25}Nb_{1.75}In_{0.25}O_{12}$ shows an opposite effect (Fig. 9b). Comparing the activation energies to those of other lithium ion conductors, such as LiPON (0.55 eV) [31], $LiZr_2(PO_4)_3$ (0.43 eV) [32], $Li_5La_3Ta_2O_{12}$ (0.56 eV) [8], $Li_6SrLa_2Nb_2O_{12}$ (0.50 eV) [14], $Li_6BaLa_2Nb_2O_{12}$ (0.44 eV), $Li_6BaLa_2Ta_2O_{12}$ (0.40 eV) [15], and $Li_{3+x}(V_{1-x}Ge_x)O_4$ ($x = 0.8$: 0.53 eV) [33], we see that all activation energies obtained for the ionic conduction of garnet-like compounds are comparable to other fast lithium ion conductors. However, it is slightly higher than that of the best-known fast lithium ion conducting perovskite-type structured $(Li,La,\square)TiO_3$ (0.40 eV) [26], $Sr_{0.5}La_{0.05}Li_{0.35}\square_{0.10}Ti_{0.5}Ta_{0.5}O_3$ (0.33 eV) [28] and $Nd_{0.56}Li_{0.33}TiO_3$ (0.46 eV) [34].

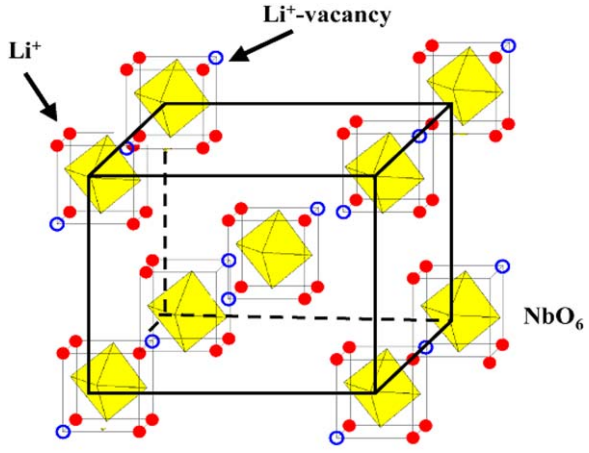


Fig. 6. Idealized 1/8th of crystal structure of garnet-like $Li_5La_3Nb_2O_{12}$. The $NbO_6$ octahedrons are surrounded cubically by six lithium ions and two vacant lithium sites [9] (schematic).

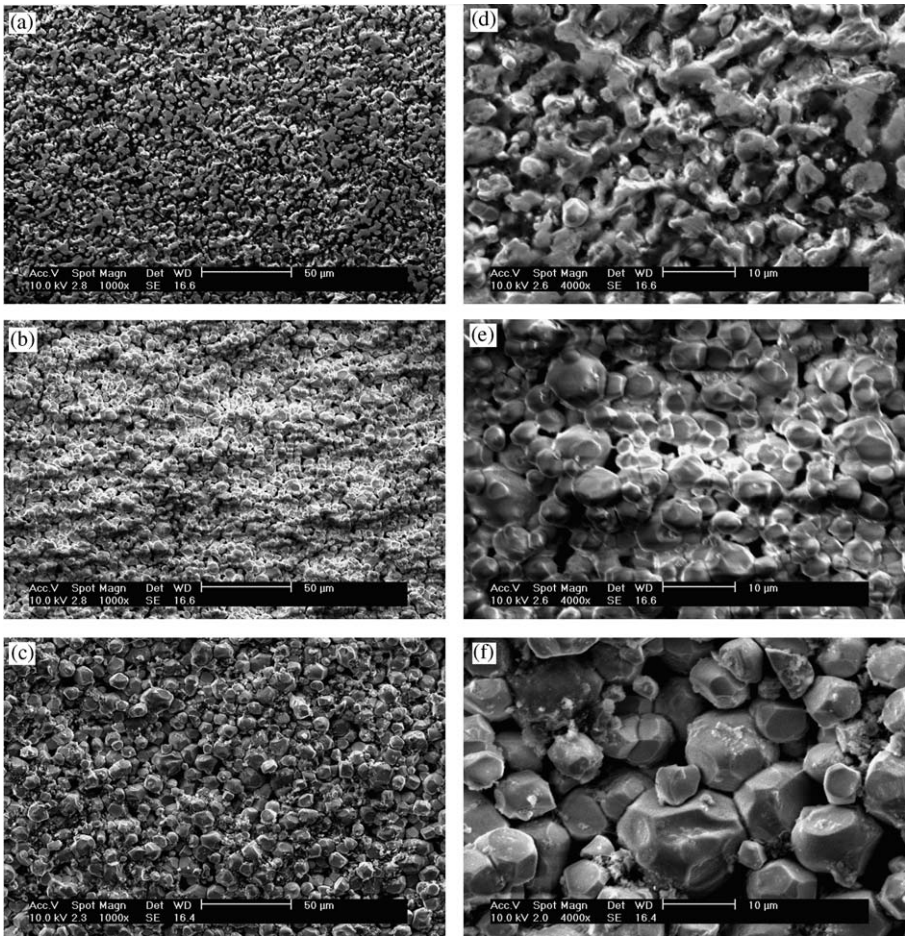


Fig. 7. SEM images of $Li_5La_3Nb_2O_{12}$ sample prepared at (a) 900 °C (LLNO-1), (b) 950 °C (LLNO-2), and (c) 1000 °C (LLNO-3). (d)–(f) Show the same in higher magnifications. We see that the grain size increases with increasing sintering temperature.

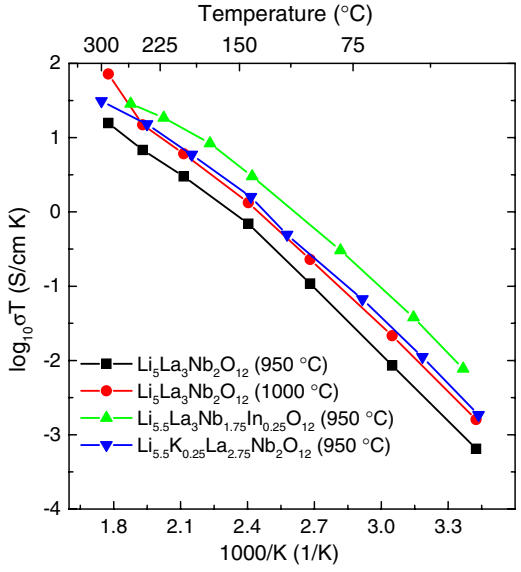


Fig. 8. Comparison of lithium ion conductivity of the best conducting In- and K-doped garnet-related compounds (LLNIO-2 and LLKNO-2) investigated in the present work. For comparison, the conductivity data of the parent compound $Li_5La_3Nb_2O_{12}$ prepared at 950 °C sample is shown along with the 1000 °C sample.

## 5. Conclusions

Substitution of In for Nb and K for La in $Li_5La_3Nb_2O_{12}$ yields new members of garnet-like materials. The lattice parameter increases with the substitution of larger size trivalent In-ions for smaller sized pentavalent Nb ions. For example, substitution of $In^{3+}$ ($r_{CN6}$: 0.79 Å) for $Nb^{5+}$ ($r_{CN6}$: 0.64 Å) ion shows an increase in the lattice parameter ($Li_5La_3Nb_2O_{12}$: 12.8005(9) Å; $Li_{5.5}La_3Nb_{1.75}In_{0.25}O_{12}$: 12.826(1) Å for 1000 °C sintered sample). The lattice parameter was found to decrease with increase in the sintering temperature for the parent compound $Li_5La_3Nb_2O_{12}$, while In- or K-doped materials show an opposite effect. Garnets prepared at high temperature exhibit higher ionic conductivity than that prepared at low temperature, which has been explained with help of microstructure. The electrical conductivity increases with substitution of In and K in $Li_5La_3Nb_2O_{12}$. Among the investigated compounds, the In-substituted $Li_{5.5}La_3Nb_{1.75}In_{0.25}O_{12}$ sample prepared at 950 °C exhibits the highest bulk ionic conductivity of $1.8 \times 10^{-4}$ S/cm at 50 °C. The activation energy for the lithium ion conductivity falls in the range 0.49–0.56 eV for the investigated compounds. The diffusivity obtained from

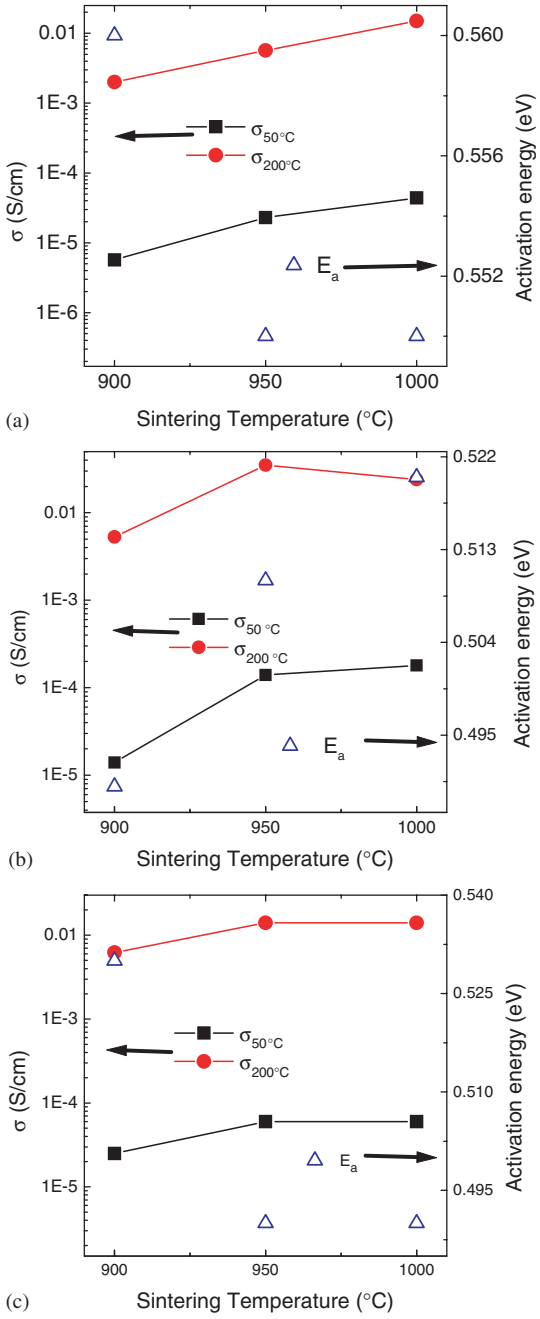


Fig. 9. Sintering temperature dependencies of the electrical conductivity and activation energy of (a) $Li_5La_3Nb_2O_{12}$, (b) $Li_{5.5}La_3Nb_{1.75}In_{0.25}O_{12}$, and (c) $Li_{5.5}La_{2.75}K_{0.25}Nb_2O_{12}$.

the AC conductivity and powder XRD data lies in the range $10^{-10}$–$10^{-7}$ $cm^2/s$ over the temperature regime 50–200 °C, which is quite a large for the solid state and comparable with liquids.

## Acknowledgments

The authors thank Mr. A. Siddiram and Mr. M. Sakithivel for their assistance in the preparation and SEM investigation of samples, respectively. Dr. Thangadurai thanks the DAAD, Bonn for the financial support.

## References

[1] A.D. Robertson, A.R. West, A.G. Ritchie, Solid State Ionics 104 (1997) 1–11.
[2] (a) G.Y. Adachi, N. Imanaka, H. Aono, Adv. Mater. 8 (1996) 127–135;
(b) T. Kudo, in: P.J. Gellings, H.J.M. Bouwmeester (Eds.), The CRC Handbook of Solid State Electrochemistry, CRC Press, London, 1997, p. 195;
(c) C. Julien, in: P.J. Gellings, H.J.M. Bouwmeester (Eds.), The CRC Handbook of Solid State Electrochemistry, CRC Press, London, 1997, p. 371.
[3] C. Julien, G.A. Nazri, Solid State Batteries: Materials Design and Optimization, Kluwer Academic Publications, Boston, 1994.
[4] H. Aono, N. Imanaka, G.Y. Adachi, Acc. Chem. Res. 27 (1991) 265–270.
[5] J.T.S. Irvine, A.R. West, in: T. Takahashi (Ed.), High Conductivity Solid Ionic Conductors, Recent Trends and Applications World Scientific, Singapore, 1989, p. 201.
[6] V. Thangadurai, W. Weppner, Ionics 8 (2002) 281–292.
[7] J.B. Bates, N.J. Dudney, B. Neudecker, A. Ueda, C.D. Evans, Solid State Ionics 135 (2000) 33–45.
[8] V. Thangadurai, H. Kaack, W. Weppner, J. Am. Ceram. Soc. 86 (2003) 437–440.
[9] H. Hyooma, K. Hayashi, Mater. Res. Bull. 23 (1988) 1399–1407.
[10] D. Mazza, Mater. Lett. 7 (1988) 205–207.
[11] V. Thangadurai, S. Adams, W. Weppner, Chem. Mater. 16 (2004) 2998–3006.
[12] V. Thangadurai, W. Weppner, J. Am. Ceram. Soc. 88 (2005) 411–418.
[13] (a) V. Thangadurai, W. Weppner, Adv. Funct. Mater. 15 (2005) 107–112;
(b) V. Thangadurai, W. Weppner, J. Power Sources 142 (2005) 339–344.
[14] R.H. Mitchell, Perovskites Modern and Ancient, Almaz Press Inc., Ontario, 2002.
[15] A.F. Wells, Structural Inorganic Chemistry, fifth ed., Clarendon Press, Oxford, 1984.
[16] R.W.G. Wyckoff, Crystal Structures: Inorganic Compounds $R_x(MX_4)_y$, $R_x(M_nX_p)_y$, Hydrates and Ammoniates, vol. 3, second ed., Interscience Publishers, New York, 1960.
[17] R.D. Shannon, Acta Crystallogr. A 32 (1976) 751–767.
[18] G.S. Lewis, A. Atkinson, B.C.H. Steele, J. Drennan, Solid State Ionics 152–153 (2002) 567–573.
[19] P.J. Scanlon, R.A.M. Bink, F.P.F. Van Berkel, G.M. Christie, L.J. Van Ijzendoorn, H.H. Brongersma, R.G. Van Welzenis, Solid State Ionics 112 (1998) 123–130.
[20] V. Thangadurai, R.A. Huggins, W. Weppner, J. Power Sources 108 (2002) 64–69.
[21] J.T.S. Irvine, D.C. Sinclair, A.R. West, Adv. Mater. 2 (1990) 132–138.
[22] J.E. Bauerle, J. Phys. Chem. Solids 30 (1969) 2657–2670.
[23] X. Xu, Z. Wen, Z. Gu, X. Xu, Z. Lin, Solid State Ionics 171 (2004) 207–213.
[24] (a) Y. Kobayashi, H. Miyashiro, T. Takeuchi, H. Shigenura, N. Balakrishnan, M. Tabuchi, H. Kageyama, T. Iwahori, Solid State Ionics 152–153 (2002) 137–142;
(b) C.H. Chen, S. Xie, E. Sperling, A.S. Yang, G. Henriksen, K. Amine, Solid State Ionics 167 (2004) 263–272.
[25] (a) K. Yamajii, T. Horita, N. Sakai, H. Yokokawa, Solid State Ionics 152–153 (2002) 517–523;
(b) C. Haavik, E.M. Ottesen, K. Nomura, J.A. Kilner, T. Norby, Solid State Ionics 174 (2004) 233–243.
[26] Y. Inaguma, C. Liquan, M. Itoh, T. Nakamura, T. Uchida, H. Ikuta, M. Wakihara, Solid State Commun. 86 (1993) 689–693.
[27] Y. Inaguma, T. Katsumata, M. Itoh, Electrochemistry 6 (2000) 534–536.

[28] P. Maldonado-Manso, E.R. Losilla, M. Martinez-Lara, M.A.G. Aranda, S. Bruque, F.E. Mouahid, M. Zahir, Chem. Mater. 15 (2003) 1879–1885.
[29] H. Rickert, Electrochemisty of Solids An Introduction, Springer, Berlin, 1982.
[30] W. Weppner, in: P.J. Gellings, H.J.M. Bouwmeester (Eds.), The CRC Handbook of Solid State Electrochemistry, CRC Press, London, 1997, p. 295.
[31] Y. Yu, J.B. Bates, G.E. Jellison, F.X. Hart, J. Electrochem. Soc. 144 (1997) 524–532.
[32] M. Cascilo, U. Costantino, L. Merlini, I.G.K. Andersen, E.K. Andersen, Solid State Ionics 26 (1988) 229–235.
[33] A.R. Rodger, J. Kuwano, A.R. West, Solid State Ionics 15 (1985) 185–198.
[34] Y. Harada, Y. Watanabe, J. Kuwano, Y. Saito, J. Power Sources 81–82 (1999) 777–781.